Cell Reports
Physical Science

CellPress
OPEN ACCESS

Article

# Solar Cogeneration of Electricity with High-Temperature Process Heat

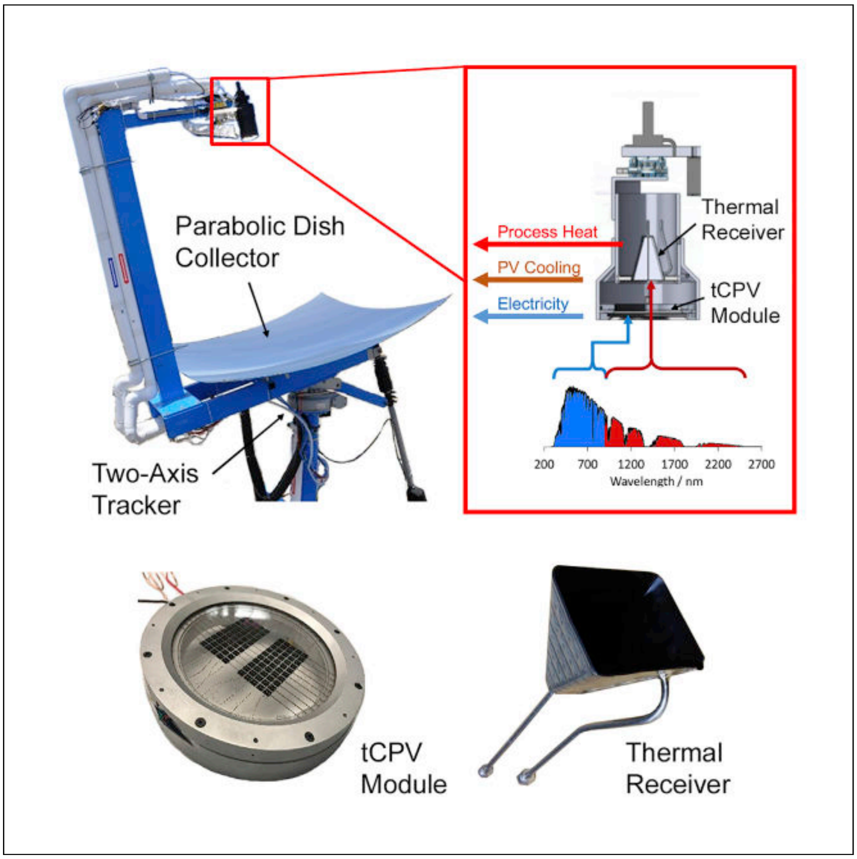


New technologies are needed to meet the growing demand for zero-net-energy and greenhouse-gas-free high-temperature process heat applications. Here, Codd and Escarra et al. demonstrate the field operation of a modular, hybrid solar converter with electricity and steam outputs, coupling concentrating photovoltaic and thermal technologies to achieve high efficiency at a competitive cost.

Daniel S. Codd, Matthew D. Escarra, Brian Riggs, ..., Jacob Platz, Naman Gupta, Fletcher Miller

codd@sandiego.edu (D.S.C.)
escarra@tulane.edu (M.D.E.)

HIGHLIGHTS

Solar cogeneration of electricity and steam demonstrated with 85.1% efficiency

Steam output reached 248°C, while average CPV cell temperatures remained <110°C

Transmissive PV module field validated for >8 h at >300 suns concentration

System levelized cost of heat of 3¢/kW$_t$h for an installation in San Diego, CA

Codd et al., Cell Reports Physical Science *1*, 100135
August 26, 2020 
https://doi.org/10.1016/j.xcrp.2020.100135

Please cite this article in press as: Codd et al., Solar Cogeneration of Electricity with High-Temperature Process Heat, Cell Reports Physical Science (2020), https://doi.org/10.1016/j.xcrp.2020.100135

Cell Reports Physical Science

CellPress OPEN ACCESS

Article

# Solar Cogeneration of Electricity with High-Temperature Process Heat

Daniel S. Codd,[1,4,5,*] Matthew D. Escarra,[2,4,*] Brian Riggs,[2] Kazi Islam,[2] Yaping Vera Ji,[2] John Robertson,[2] Christopher Spitler,[1] Jacob Platz,[1] Naman Gupta,[3] and Fletcher Miller[3]

## SUMMARY

**Side-by-side installations of flat plate photovoltaics and parabolic trough collectors consume significant space and have high system losses; by using an all-in-one, spectrum-splitting hybrid receiver, electricity and high-temperature heat can be generated with a single efficient system. Here, the performance of a transmissive concentrator photovoltaic/thermal (tCPV/T) system is demonstrated on-sun, with a total energy efficiency of 85.1% $\pm$ 3.3%, 138 W electric power at 304 suns (with average cell temperatures <110°C), 903 W hot water output (average 34°C and 1.7 bar, peak temperatures to 56°C), and 1,139 W high-temperature steam output (average 201°C and 45 bar, peak temperatures up to 248°C). The spectrum-splitting hybrid receiver uses a sparse array of III–V triple-junction solar cells on GaAs substrates contained within a transparent microchannel water cooling stack, followed by a structured flow path thermal receiver cooled with pressurized water. System economics based on a 2.72-m$^2$ prototype performance is shown to be at or near market competitiveness to natural-gas-produced process heat for a variety of locations, with a levelized cost of heat of 0.03 \$/kW$_t$h for an installation in San Diego, California.**

## INTRODUCTION

There has been a rising interest in combined heat and power systems to maximize system efficiencies and reduce operating expenses.[1–3] Many of these systems still use conventional fuels and generators and focus on power production, using waste heat for space heating or other applications. For industries such as food and beverage processing, chemical refining, and enhanced oil recovery, thermal loads are a significant portion of the overall energy budget, accounting for significant fuel costs, operation and maintenance expenses, and emissions.[4] Furthermore, these applications need high temperatures (>150°C) that are difficult to achieve through typical renewable methods. Achieving high-temperature process heat from an abundant solar resource would significantly enhance sustainability in the commercial and industrial sectors.[5–8]

Solar cogeneration has been a growing area of work, including the development of hybrid photovoltaic/thermal (PV/T) systems.[9–14] Proposed designs are based on conventional solar thermal collectors, including flat plate,[15–17] parabolic trough collectors (PTCs),[18,19] and dish systems,[20–22] with PV cells acting as thermal absorbers in a topping configuration or as spectrum-splitting optics converting a fraction of the incident light to electricity and the remainder directed to a separate thermal receiver.[23] The design

[1]Department of Mechanical Engineering, Shiley-Marcos School of Engineering, University of San Diego, San Diego, CA 92110, USA

[2]Department of Physics and Engineering Physics, Tulane University, New Orleans, LA 70118, USA

[3]Department of Mechanical Engineering, San Diego State University, San Diego, CA 92182, USA

[4]These authors contributed equally

[5]Lead Contact

*Correspondence: codd@sandiego.edu (D.S.C.), escarra@tulane.edu (M.D.E.)

https://doi.org/10.1016/j.xcrp.2020.100135

of PV/T systems often sacrifices electrical efficiency for higher temperature heat output by physically coupling cell temperature to thermal output temperature, in which cells must operate at higher temperatures than the output heat transfer fluid (HTF). To achieve thermal energy temperatures in the range of 250°C, as reported here, cells must operate at $\sim \geq 300°C$; this has been demonstrated on a small prototype scale, but it has not been fully developed into outdoor-tested hybrid systems and is limited by reduced solar cell efficiency and a lifetime at high operating temperatures.[24] Spectrum-splitting hybrid PV/T systems such as those using dichroic filters and reflectors,[18,23] nanoparticle-containing fluids,[25] or reflective thin-film silicon or gallium arsenide (GaAs) cells for spectrum splitting,[19,26] have yet to be demonstrated in full-scale, outdoor conditions with both electricity and high-temperature thermal output with similarly high conversion efficiencies. Nanofluid spectrum splitting is limited by thermally induced degradation of the nanofluids and optical splitting inefficiency, while other thin-film spectrum-splitting approaches are limited by conversion efficiency due in part to the use of PTCs. Other side-by-side solar thermal and photovoltaic plant installations, which is the current favored commercial approach, compromise both electric and thermal systems to achieve design performance by using larger footprints with less shared infrastructure.[28]

In this article, we integrate and demonstrate a system that generates solar electricity and high-temperature heat in a modular, small footprint, low cost, and high-efficiency design. We show for the first time the integration of a low-temperature PV operation with a high-temperature solar thermal operation within the same hybrid receiver. The system exploits an advanced version of a spectral-splitting transmissive concentrator photovoltaic (tCPV) module coupled to a dimple plate cavity thermal receiver, allowing for independent temperature control of PV and thermal components.[29] We fabricate and test multiple tCPV/thermal (tCPV/T) receivers on-sun, ramping the collector area from 0.25 to 2.72 $m^2$ to increase the system power and effective concentration factor. We characterize the electrical and thermal performances of the system under various outdoor conditions and HTF flow rates, achieving temperatures up to 248°C while maintaining average cell temperatures <110°C, with high overall system efficiency.

## RESULTS AND DISCUSSION

### High-Temperature Hybrid Receiver

We recently demonstrated on-sun testing of an early prototype of a spectral-splitting tCPV module.[30,31] This water-cooled module uses transmissive III–V triple-junction solar cells on GaAs substrates, with outdoor testing under concentrated sunlight showing up to 21 W electrical output, 21.5% electrical conversion efficiency (equating to 34.7% in-band conversion efficiency), and 58.8% transmission of out-of-band incident light. Here, in-band and out-of-band refer to photon energies above and below the bandgap of the GaAs substrate, respectively. These early prototype iterations were small (75 mm diameter tCPV receiver aperture and <50 cells) and were tested under relatively low input power (<900 W) for a limited duration to inform the development of the full-scale, high-performance receivers reported here.

The core innovation lies in the use of infrared (IR)-transmissive concentrator PV cells coupled with a cavity thermal receiver, allowing for separate harvesting of ultraviolet (UV)/visible and IR light[22] (Figure 1A). The advantage of spectral splitting using tCPV cells is in the simplicity, efficiency, and cost-effectiveness of the approach for CPV/T systems. Traditional spectrum-splitting methods, such as heat reflectors, prism-based splitters, holographic and dichroic filters, and liquid absorption filters, require

Please cite this article in press as: Codd et al., Solar Cogeneration of Electricity with High-Temperature Process Heat, Cell Reports Physical Science (2020), https://doi.org/10.1016/j.xcrp.2020.100135



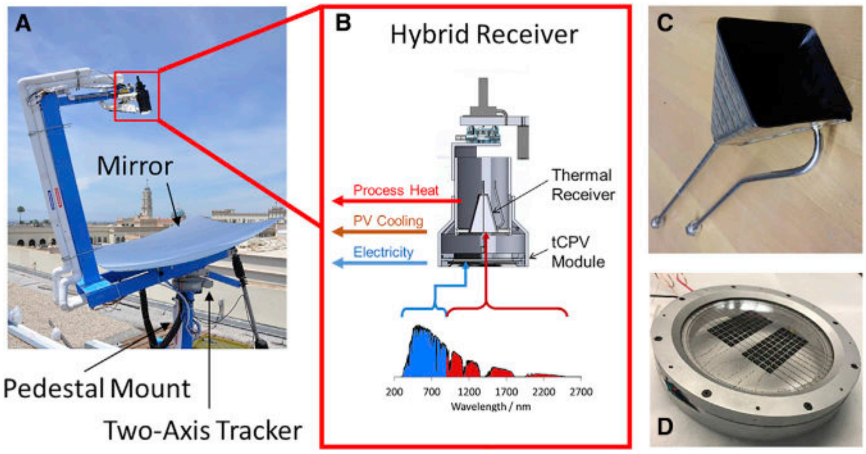


**Figure 1. High-Temperature Hybrid Solar System Overview**

(A–D) The prototype mounted at an outdoor test facility (A); schematic of the power flow through the hybrid receiver cross-section (B); and photographs of (C) cavity thermal receiver and (D) tCPV module subassemblies. Sunlight is concentrated by the paraboloidal mirror on the 2-axis tracker and directed to the hybrid receiver. There, the tCPV module converts a portion of the high-energy photons to electricity and low-temperature heat, while the balance transmits through to the thermal receiver, where it is absorbed and converted to high-temperature heat.

extra apparatus, precise alignment, and/or complex optical design. Many suffer from significant sensitivity to the angle of incidence, which is a challenge for their use in concentrating systems. Our tCPV cells serve as both electricity generators and spectrum splitters, with minimal incident angle sensitivity and no major additional components other than the requisite CPV cooling system.[32] This allows for higher system efficiency and lower cost than competing designs.[28] Prior efforts to use transmissive PV cells for spectrum splitting in PV/T systems show early-stage designs using non-concentrator (1 sun) cells.[33–37] Our system is the first to use tCPV cells and has been fully prototyped and field tested.

In our system, the hybrid receiver is located at the focal plane of a mirrored dish collector, which tracks the sun via a low-cost two-axis tracker. The system is designed to be small scale and modular, with collector areas on the order of 1–5 $m^2$ per receiver. The hybrid receiver is two-stage in design, comprising physically and thermally separated electrical PV and thermal receiver components situated along the optical axis of the collector, which allows for the operation of each converter at its desired temperature and performance level (Figure 1B). A tCPV module absorbs UV/visible light while transmitting IR wavelengths to a thermal receiver with a high-temperature, high-absorptivity coating (Figure 1C).[30,31] The tCPV module uses a spaced array of 100 III–V triple-junction cells designed in partnership with and manufactured by Boeing-Spectrolab to operate between 500 and 1,000$\times$ at an $\sim$48% conversion efficiency for in-band light.[29] The cells are arranged in a 143-mm diameter window aperture sized for the negligible spillage of sunlight onto the receiver's aluminum collar (Figure 1D). Approximately 71% of out-of-band light, conventionally wasted as heat or otherwise not captured, is transmitted through the cell.[29,32] Each cell is 5.5 $\times$ 5.5 mm with a total area of 0.3025 $cm^2$, measured by digital calipers and optical microscopy. The tCPV module uses a transparent microfluidic cooling system to maintain module operation temperatures <110°C.[38] The tCPV cooling energy can be harnessed as a secondary thermal energy stream for low-temperature heat applications. The light that transmits through or bypasses the CPV cell array falls on a cavity pillow plate thermal receiver painted with Pyromark 2500 (Figure 1C). This unique

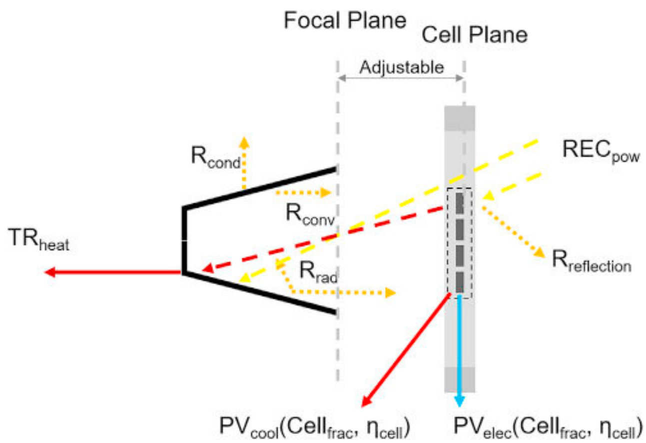


**Figure 2. Solar Cogeneration Design Parameters: Power Flow and Performance Schematic for the 2-Stage tCPV/T Receiver**

The distance between the cell plane and the focal plane is adjustable, and by doing so, the ratio of PV electrical and thermal receiver output can be tuned. $REC_{pow}$ refers to the total power incident on the hybrid receiver; $Cell_{frac}$ and $\eta_{cell}$ refers to the fraction of receiver power incident on cell array and the full-spectrum efficiency of the cells, respectively; $R_{reflection}$ refers to the optical losses from the front surface of the tCPV module due to reflection; $R_{cond}$, $R_{conv}$, and $R_{rad}$ refer to thermal losses in the thermal receiver due to conduction, convection, and radiation, respectively, which are largely suppressed or absorbed by the tCPV module; and $PV_{elec}$, $PV_{cool}$, and $TR_{heat}$ refer to the 3 output power streams, PV electrical, PV cooling, and thermal receiver, respectively (see Note S1).

laser welded and hydraulically inflated mesoscale thermal receiver enables efficient (>90%) light capture and heat transfer to the HTF that flows through the walls of the receiver and exits the system for process heat applications.[39,40] This design results in three usable output power streams to maximize system exergy (see Note S1): electric power, low temperature (<100°C) heat, and high temperature (>100°C) heat.

## Solar Cogeneration Design Parameters

As shown in previous work, solar industrial process heat (SIPH) can become cost competitive with the addition of solar electric power output.[28] This creates a need to balance the electrical and thermal outputs (Figure 2). The optical performance of the tCPV module will greatly affect the power that the thermal receiver receives. Because of this, thermal power of the high-temperature thermal stream is the first design parameter specified. Next, the tCPV module is designed from an optical perspective, considering transmission losses due to its components (e.g., cells, substrates, cooling, wiring), with the tCPV cells contributing the most to power diverted away from the thermal receiver.[22,32] As the thermal receiver is last in the power flow of the system and is thermally decoupled from the tCPV components, its performance can be maximized without significant concern for the tCPV module. Thermal receiver convective losses are nearly eliminated due to the presence of the tCPV acting as an aperture window. Radiative heat gain back to the tCPV module is minimal, as a majority of this energy that is not absorbed in the microfluidic cooling channels of the tCPV module will transmit through the IR-transparent tCPV cells.

We carried out modeling to gain insights into the present experiment and future performance. Using an optical model based on measured direct normal irradiance (DNI), known receiver shadowing losses, reflectivity measurements of the dish, and the measured flux profile on the receiver (see Experimental Procedures), the maximum power incident on the cell array is determined. With these power inputs, the tCPV module electrical and cooling systems are modeled. A microfluidic heat

Cell Reports
Physical Science
Article

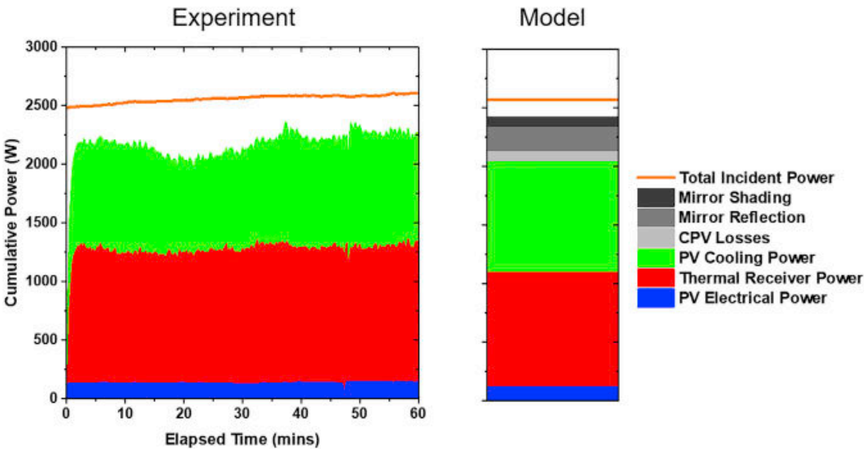


**Figure 3. Hybrid System Performance: Power Generation during On-Sun Field Testing**
Experimental performance showing the distribution of tCPV electric, thermal receiver (steam), and tCPV cooling (hot water) output power during a 1-h outdoor test. The expected performance for this system test based on measurements of individual components is shown at right.
See also Figure S3.

transfer model is used to determine the maximum power that an individual cell can absorb while remaining below the maximum allowed cell and module operating temperature of 110°C.[38] Thermofluidic modeling was used to predict the cell temperature based on the incoming solar power, cell optical properties, cell efficiency, and the thermal properties of the module stack, with the microfluidic cooling channel as a fixed temperature sink, varying from cell to cell in the streamwise direction based on flow properties and expected heating from previous cells in the same channel. Then, flux map analysis (see Figure S2) is used to determine the concentrator focal point and tCPV plane spacing necessary to achieve this limit. Flux map analysis is combined with maximum power point and cell-cooling models to predict the average concentration over each cell in the array and its associated operating temperature, current, and voltage. The electrical model also incorporates series resistance losses, current mismatch losses, and optical reflection losses. Knowing the expected operating current and voltage of each cell, the tCPV circuit can be designed to minimize current and voltage mismatch and resistive losses.[30] This leads into mechanical system design, packaging, and integration with the thermal receiver.

## Hybrid System Performance

Figure 3 shows the power distribution for a long-duration test of our 9$^{th}$ tCPV module and 3$^{rd}$-generation thermal receiver with a fully unmasked dish (100% of target operating flux with an average DNI of 941 W/m$^2$), with 33.8°C and 220.7°C average outputs for the PV cooling and high-temperature streams, respectively, alongside the modeled power distribution. Of the total incident power, 11.5% (see Note S1) is lost before reaching the hybrid receiver from optical losses due to shading from the tracker arm and receiver and reflectivity of the mirror. The total collection efficiency (output power/total incident power) from the thermal receiver, tCPV electric power, and tCPV cooling is 85.1% $\pm$ 3.3%. Losses from the front side of the tCPV module are modeled at 4.1%, which includes reflection losses of 3.5% and thermal losses of 0.6%. Independently, the electric power, tCPV cooling, and thermal receiver heat make up 5.4% $\pm$ 0.2%, 35.2% $\pm$ 2.1%, and 44.5% $\pm$ 2.6% of the total dish incident power, with a total average power capture of 2,180 W. The average power output for electricity, hot water, and high-temperature steam is 138 $\pm$ 5, 903 $\pm$ 45, and 1,139 $\pm$ 57 W, respectively. Uncertainty is larger for the thermal streams due to inherent error limits in the flow rate and temperature measurement.

An integrated system model was developed to predict and validate the total thermal and electrical output and the losses from system components. The integrated model used inputs from each experimentally validated subsystem model, including optical performance of the paraboloidal dish, photovoltaic module efficiency, photovoltaic module optical behavior, and thermal receiver efficiency. The model tracks input to output power from each component along the optical path (Figure 1), accounting for all of the loss mechanisms at each step. Our modeled system performance is in good agreement with these experimental values for the same DNI. Tables S1–S3 show the key performance metrics for several extended outdoor testing campaigns of these hybrid tCPV/T receivers (the aforementioned full power data are denoted by test #1; tests are numbered in reverse order from initial low power, partially masked mirror trials to full power runs).

As presented for test #1 (Figure 3), thermal losses are essentially negligible if the tCPV cooling waste heat stream is harvested. However, there is non-zero thermal transport between the high-temperature receiver and the tCPV module. The thermal receiver is shielded by the tCPV module and well insulated. The primary loss mechanism for the inverted cavity thermal receiver is long wavelength radiation out of its small aperture to the backside of the PV module. This energy is absorbed within the tCPV module cells, substrate, and cooling channels (see Figure S2), adding to the thermal load on the tCPV module, and transferred to the low-temperature heat collection stream. The actively cooled tCPV module is subject to radiation, convection, and conduction losses to its surroundings. However, primary heat generation and extraction occurs within and near the cell layer and the module front side is relatively cool, support interfaces are kept as small as possible, and subsequent thermal losses are low. Obviously, operating the tCPV module at higher temperatures to enhance the usefulness of the low-temperature thermal stream will result in increased losses, but these are still relatively small (e.g., PV module front side at 100°C results in 63 W convective and 19 W radiative losses, which are 3.2% of the total system input power) and remain within the uncertainty associated with measured power flows.

## Optical Performance

The optical performance of the tCPV module dictates the system power distribution.[32] Reflection off, and any spillage outside, the front window leads to absolute power loss, while full solar spectrum transmission affects how much light will reach the thermal receiver. Because of this, a full optical characterization of the optoelectronic stack was conducted before integrated testing to allow for predictive performance modeling. A transfer matrix-style method is used to calculate the transmission through each planar layer of the module. Shadowing from copper wires and reflection at the front and back sides of the CPV cells are included. The tCPV module is broken into three unique regions based on the materials within that cross-section: cell, bypass with channels, and bypass without channels. The region-specific transmission spectra can be found in Figure S1. Combined with spatial flux mapping of the concentrator dish at the tCPV plane (65 mm inboard of the dish focal point), the total power reflected, transmitted, and absorbed in the tCPV module can be predicted (Table 1). Figure S2 shows an overlay of the measured spatial flux map, with tCPV module regions labeled and their cross-sections illustrated.

**Table 1. Optical Power Distribution across the tCPV Module Regions**

| | Absorbed | Reflected | Transmitted | Total Power |
|---|---|---|---|---|
| Bypass, no channel | 0.004 | 0.025 | 0.338 | 0.367 |
| Bypass, channel | 0.014 | 0.022 | 0.224 | 0.260 |
| Cell stack | 0.241 | 0.059 | 0.074 | 0.373 |
| Total | 0.259 | 0.105 | 0.636 | 1.000 |

tCPV, transmissive concentrator photovoltaic.

## Electrical Performance

Intermittent current-voltage (IV) sweeps were taken throughout the duration of each outdoor test, while two-terminal output power at an estimated maximum power point was monitored between sweeps. Figure 4 shows a typical IV sweep from the test data, here, with a 17% masked dish (83% of target operating flux with average DNI of 705 W/m$^2$). The total module electrical efficiency, $\eta_{mod}$, is measured as 24.7%, in which $\eta_{mod}$ = (electrical power output of module)/(power incident on cell area). Since each cell is designed to absorb only the light of energy above the band gap of GaAs and transmit lower energy light, we also quantify electrical performance by in-band module efficiency, defined as $\eta_{mod}^{inband}$ = (power output of module)/(power of $\lambda$ < 873 nm incident on cell area). The in-band module efficiency is measured at 39.9%. The module efficiency values have the potential to be improved to 27.0% and 43.8% for full spectrum and in-band, respectively, by using more efficient transmissive photovoltaic cells.[30] These cells have already been demonstrated independently and may be used in future system iterations.[29]

## tCPV Cooling Performance

One critical design requirement is the ability to maintain the photovoltaic cells below 110°C to prevent accelerated degradation and catastrophic failure. To do this, a transparent microfluidic cooling system was developed to extract waste heat from the tCPV cells while allowing significant optical flux to reach the thermal receiver.[38] Predictive modeling of the tCPV module shows that the total thermal resistance of the cooling system should be 12.6 K/W and should result in a maximum cell temperature of 87°C with a mean temperature of 66°C. Experimental tCPV module cell and cooling fluid temperatures were monitored for all of the tests (Figure 5). The outlet temperature of the tCPV cooling fluid can be adjusted by tuning the mass flow rate of the fluid and was measured as high as 55.6°C (see Table S3). For the duration of the 60-min, 100% target operating flux test, the average cell temperature does not rise above the threshold value of 110°C (Figure 5D).

In addition to monitoring average cell temperatures, one can also review individual thermocouple measurements, as reported in Figure 5C, to determine the relative spread of cell temperatures. It is important to note that with a limited number of thermocouples, this analysis may miss some localized hotspots. The location of the hotspots on the module also varies throughout the day due to the position of the sun, orientation, and subsequent elastic deflection of the tracker, mirror and receiver support structure, and variable wind loads. The sensor labeled PV TC1 in Figure 5C demonstrated higher temperatures than others throughout the testing campaign. Several factors may have contributed to this discrepancy, including higher local flux, installation near an isolated cell with poor performance, embedded thermocouple error, poor adhesion, and assembly inhomogeneity. The latter may indeed be expected with a resultant thermocouple air bubble-bolometer effect in the hand-built prototype; a post-test analysis did not show significant degradation

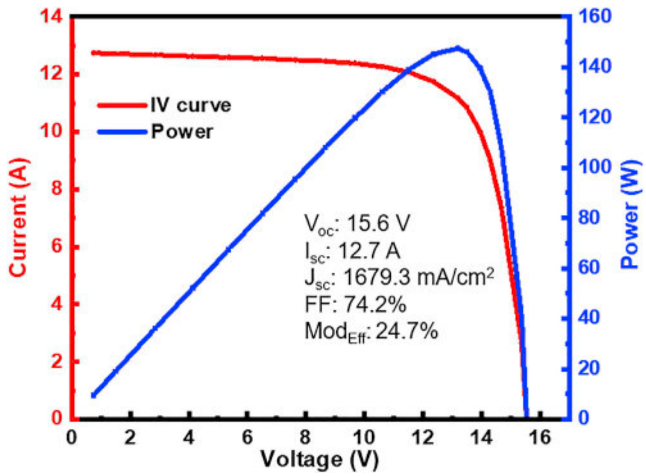


**Figure 4. Electrical Performance of the tCPV Module during On-Sun Testing**
Representative current versus voltage (IV) and power versus voltage curves captured at an average concentration of 252 suns.

near TC1 as compared to the other regions. Similarly, sensors TC2 and TC6 exhibited lower than expected temperatures, possibly due to location offsets closer to the water microchannels. Bubbles within the polydimethylsiloxane (PDMS) encapsulant were observed on both the front and back layers, attributed to the prototype fabrication process and the lack of use of a PDMS adhesion agent. Mismatches between the measured and modeled cell temperatures are due to prototype fabrication defects within the tCPV module, such as delamination of the encapsulant layers, and are discussed in detail elsewhere.[38] Due to these prototyping and data-capture limitations, average temperatures were used to assess cooling performance and serve as tracker alarm triggers should cooling system failure occur.

## Thermal Receiver Performance

The thermal receiver consists of thin sheets of corrosion-resistant alloy that are seam welded, formed, and expanded to create a thermoplate heat exchanger with a millimeter-scale serpentine flow path. The inner surface is covered with a high absorptivity coating (Pyromark 2500), and the entire system, including HTF piping, is well insulated. The cavity-shaped thermal receiver is cooled with pressurized water as the HTF, maintaining the single-phase flow.

Initially, we developed simplified thermoplate heat exchangers to evaluate formability, weld process parameters, and thermofluidic performance. The results from these devices were incorporated into the design of the cavity receiver prototypes, with apertures ranging from 38 to 63 mm. In conjunction with a laser welding service provider, we have developed tooling and fixtures to enable their production. Typical devices were fabricated from 0.5-mm-thick Inconel 625 sheets, with 1 × 10 mm nominal flow path channels and a series of inline 2.5-mm diameter spot welds, added for structural rigidity during the hydraulic inflation process (240 bar) and stability during operation. Total power on-sun was varied up to 2.5 $kW_t$ using 40–50 bar (580–725 psi) pressurized water with flow rates from 0.3 to 3.0 g/s, with a Reynolds number of <1,000 in all of the cases. Designs were characterized using thermofluidic modeling, lab electrical heating rigs, and outdoor on-sun testing, instrumented with numerous rear surface-welded and immersed flow thermocouples. In addition, the thermal receiver was tested in both the hybrid configuration with the tCPV

Please cite this article in press as: Codd et al., Solar Cogeneration of Electricity with High-Temperature Process Heat, Cell Reports Physical Science (2020), https://doi.org/10.1016/j.xcrp.2020.100135



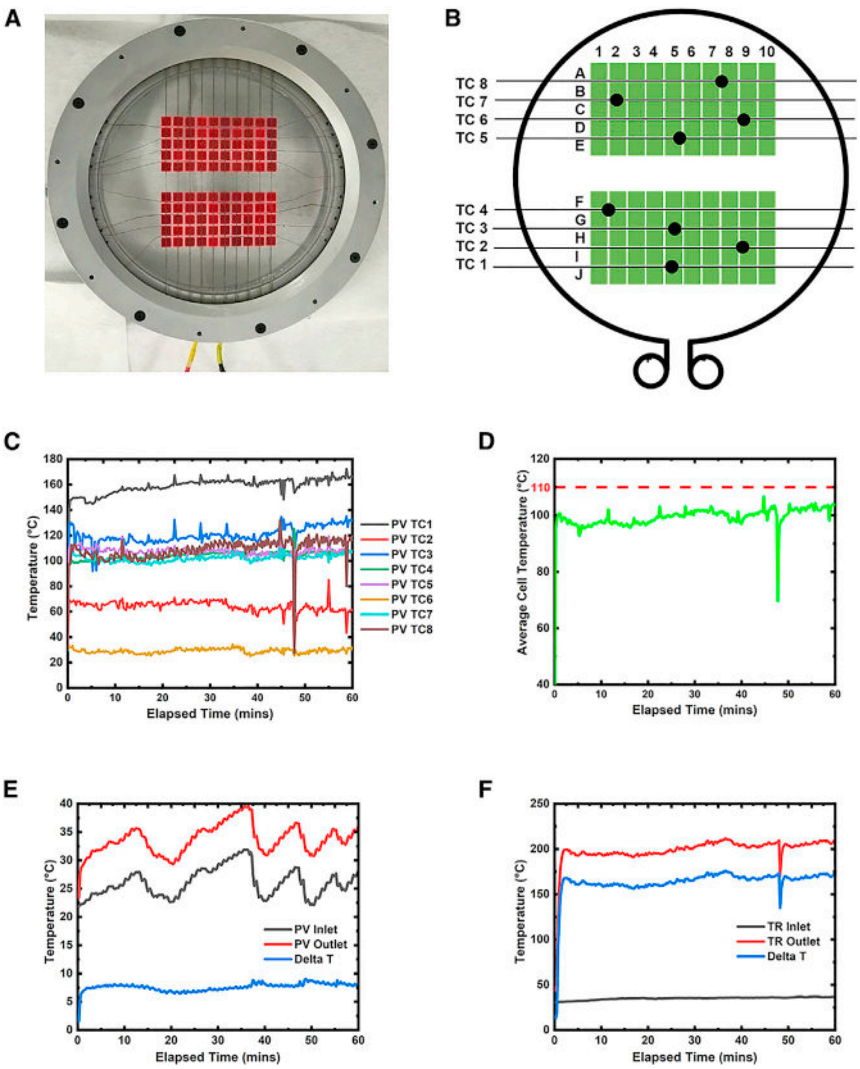


**Figure 5. tCPV Hybrid Receiver Cooling Performance and Measured Subsystem Temperatures during Outdoor Testing**

(A) Photograph of the tCPV module with cells in forward bias.

(B) Schematic of the tCPV module showing the embedded thermocouple locations; subsystem temperature data for the test shown in Figure 3, with 100% open area (full dish flux) and DNI of 941 W/m$^2$.

(C) Cell temperature data from the 8 thermocouples embedded within the 9$^{th}$ tCPV module.

(D) Average cell temperature.

(E) Temperature of the PV cooling inlet and outlet.

(F) Temperature of the thermal receiver inlet and outlet.

module installed and the thermal-only mode without any devices or covers in front of the thermal receiver aperture. The temperatures of the thermal receiver inlet and outlet were recorded and used to compute the sensible heat gain of the HTF. (Figure 5F depicts these temperatures for the hybrid test shown in Figure 3.)

The compact thermal receiver performed very reliably, and the flow path Nusselt number, and subsequent heat transfer coefficient, was found to be 2.5 times greater than the analytical value for fully developed laminar flow within similarly sized rectangular channels.[39,40] Accordingly, the bulk of energy that passes through the tCPV aperture is absorbed by the thermal receiver. The thermal receiver capture efficiency (see Note S1) is a function of the HTF temperature; in the thermal-only mode, the highest capture efficiency was measured at 89.5% at 160.9°C (see Figure S4); in the hybrid mode with tCPV module installed and serving to reduce losses, the capture efficiency is predicted to approach 92% at a maximum design outlet temperature of 250°C.

## Solar Cogeneration Technoeconomic Model and Applications

A growing focus on zero-net-energy (ZNE) within the public sector has spurred new efforts to replace energy consumption from conventional sources. Most of these efforts focus on replacing grid electrical power, building heating and cooling, and other residential and commercial energy-consuming operations through renewable electricity and hot water generation. However, there is a rising demand for technology that is able to directly reduce heating fuel demands for higher-temperature (>60°C) applications such as food pasteurization, district heating and cooling, hospital applications, chemical processing, clean water generation, paper production, and others. California's Long-Term Energy Efficiency Strategic Plan specifically calls for new commercial construction to be ZNE by 2030.[41] For the innovation to be practical, cost competitiveness is necessary.

As a case study, we examined the technoeconomic viability of the proposed system in San Diego, California. Based on the experimentally validated power output for this hybrid system in a configuration featuring 8 dishes and 8 receivers mounted on a single tracker, a typical day in San Diego would result in 4.24 kWh electric and 17.6 kWh process heat. Given this output, it would take ~88 dishes of the prototype scale (11 of these 8-dish units) to displace 80% of the total heat use and 20% of electricity use for a typical local craft brewery with a 20-barrel steam brewhouse. In this instance, solar-generated heat is well aligned with daytime-shift thermal brewing demands, and the solar-thermal fraction of total system output is high, with minimal buffer storage requirements. Electrical loads are dominated by continuous mechanical refrigeration; a low solar-electric generation fraction is desired to offset daytime electrical demand. For other users, a higher electrical fraction may be achieved with an increased CPV cell fraction, coupled with extended duration thermal and electrical storage.

The measured outdoor system performance is used in conjunction with a previously developed technoeconomic analysis methodology for combined heat and power solar systems to determine the levelized cost of heat of this system.[28] The technoeconomic model considers the net electrical and thermal efficiency of the system as well as the economic and solar resource factors for distinct regions, including US states and international sites, to determine the levelized cost of heat (LCOH) in US dollars (USD)/kW$_t$h. The model uses the average annual DNI of a region, efficiency of the system, and expected annual performance degradation to determine thermal and electrical outputs for up to 30 years of operation. The LCOH model uses a standard levelized cost of energy calculation, with the added feature that it uses electrical output and regional cost of electricity to reduce the annual cost of the system (see Note S1). Using regional commercial natural gas and electricity pricing, policies, and solar resources for an example market around San Diego, California shows that LCOH is estimated to be 3.0¢/kWh, ~6% lower than the local natural gas prices in 2019.

For a global perspective, we can look at several other locations where concentrated solar energy has historically had a foothold for the comparative location-dependent cost competitiveness of this technology (Table 2). The hybrid system installed in

Table 2. LCOH Given the Current Performance of the tCPV/T System

| Country | Average DNI ($kW_th/m^2/day$) | Electricity Rate (¢/$kW_eh$) | Natural Gas Rate (¢/$kW_th$) | tCPV/T LCOH (¢/$kW_th$) | Price Change (%) |
|---|---|---|---|---|---|
| Australia | 8.2 | 51.0 | 6.3 | 1.1 | −83 |
| Spain | 6.0 | 10.5 | 7.8 | 8.4 | 6.5 |
| Chile | 9.5 | 8.5 | 2.4 | 5.1 | 115 |
| India | 6.0 | 9.0 | 4.0 | 8.5 | 114 |

LCOH calculated for various locations, along with price change relative to local natural gas prices. Technoeconomic analysis does not assume any federal- or state-based tCPV/T subsidies for these locations. DNI, direct normal irradiance; LCOH, levelized cost of heat; tCPV, transmissive concentrator photovoltaic/thermal.

these areas, with excellent solar resources and high energy costs, could provide solar heat and power near, or even below, in the case of Australia, current natural gas pricing.

## Analysis

The demonstration of a new hybrid solar energy technology with high efficiency in field conditions, capturing system behavior in varying operating schemes and for extended durations, is a major milestone for any solar conversion technology. Most previously reported CPV/T systems aim to maximize the electrical output fraction, with the intent to compete against conventional 1-sun PV. This system is intended not to compete head to head with flat-panel PVs for renewable electricity, but rather can make a major impact in providing commercially viable sources of renewable high-temperature thermal energy. The system is very competitive in this space because of the (1) inherent modularity, (2) lower LCOH due to the subsidy of high-value electricity, and (3) overall high efficiency. Our group has performed an extensive technoeconomic analysis, accounting for the cost of the system, including III–V GaAs cells, informing the designed electrical versus thermal output fractions for various markets and applications.[28]

As with any hybrid system, load matching can be a concern if renewable hybrid fraction and delivery are not well matched with demand. Partial offsets of conventional generation with this system are a viable use case, such as in the aforementioned brewery case study with daytime-shift brewing cycles. Ultimately, higher penetration will benefit from electrical storage and/or thermal energy storage, such as steam accumulators or other longer-duration solutions. The increased adoption of such SIPH devices can reduce fuel usage in many industrial segments, including chemical production and food processing plants. Feasibility depends on high solar resources at or near the end user and available space for collectors and storage. Kurup and Turchi[4] analyzed applications in the southwestern United States and found that the potential of SIPH far exceeded the demand for the largest industrial segments within California. In addition, they noted that pressurized water or steam SIPH systems, with temperatures ranging from 120° to 220°C, were the most attractive for target markets. Installations must account for thermal transport losses; even medium-sized SIPH systems may have piping runs on the order of hundreds of meters. The modular footprint of our device may allow for closer coupling of the collection field to the end user, reducing these losses as individual modules are located closer to the factory floor. Future efforts must further investigate thermal energy storage optimized for this temperature regime and set of SIPH applications.

To meet application-specific energy demands, the system demonstrated here has the key benefit that it is configurable for varying electrical/thermal fractions.

CellPress OPEN ACCESS

Cell Reports Physical Science
Article

Electrical output can be increased by (1) using higher-performance transmissive cells, such as those previously demonstrated[29]; (2) the transmissive PV module can be built with increased cell density; or (3) the transmissive PV module can be moved along the optical axis of the concentrator toward the focal plane. The latter approach may be the riskiest, as the increased flux on the cells may necessitate better PV module cooling or cells that can operate at higher temperatures, such as those previously demonstrated using the same materials to operate at 400°C with minimal degradation.[24] This system has been modeled up to a maximum of 20% electrical output fraction, with resultant thermal fractions of 30% low-temperature tCPV cooling waste heat and 33% high-temperature heat. To accomplish this, the fraction of flux on the module that is intercepted by cells is increased from 37% to 75%. This is accomplished by increasing the cell density; the cells per module are increased from 100 to 228, and the spacing between cells is decreased from 1.0 to 0.2 mm. The impact of additional voltage and current mismatch losses otherwise using the same wiring scheme is included, and the model confirms that cell temperatures remain at less than the 110°C limit when using the highest-performing tCPV cells we have made.[31] In addition, we can improve the cooling performance of these tCPV modules. Modeling shows that a thicker microchannel would further decrease the cell temperatures by up to 10°C.[38] There is a minor trade-off, however, as a thicker microchannel would absorb more light in the water and PDMS bypass regions, which would otherwise be transmitted to the thermal receiver.

The dish concentrator offers several benefits relative to parabolic trough or non-concentrating PV/T solar electric-thermal devices: (1) the optical efficiency of a dish concentrator exceeds that of parabolic troughs or linear Fresnel systems with skew ray losses; (2) the small focal length dishes are inherently modular; and (3) dish concentrators with resultant small area point focus receivers enable cost-efficient use of high-performance materials, higher overall conversion efficiency, and attainment of higher-temperature thermal output, as demanded by some use cases. The latter is not the case for parabolic trough-based spectral splitters using linear receiver elements.[19]

By using the full range of wavelengths of sunlight, this integrated system, demonstrated on-sun, achieves 85.1% $\pm$ 3.3% efficient solar energy conversion to electricity, low-temperature hot water (tested up to 56°C), and high-temperature steam (tested up to 248°C) energy streams, all at a LCOH that is competitive with natural gas prices. With further development, this technology may provide a key solution to address zero-net-energy goals for industrial and commercial applications. The spectrum-splitting tCPV module allows the physical, electrical, and thermal separation of disparate concentrator photovoltaic and solar thermal technologies, enabling optimal performance in each subsystem. This decoupling results in higher solar collection efficiencies and thermal outlet temperatures than previously achieved in hybrid CPV/T systems, while still sharing the same solar collection infrastructure (mirror, tracker, foundation) and footprint. These advancements open the potential for renewable energy to more fully penetrate high-temperature industrial and commercial process heat markets, displacing a significant amount of conventional fuel use and carbon emissions.

## EXPERIMENTAL PROCEDURES

### Resource Availability

#### *Lead Contact*

Further information and requests for resources should be directed to and will be fulfilled by the Lead Contact, Daniel Codd (codd@sandiego.edu).

Please cite this article in press as: Codd et al., Solar Cogeneration of Electricity with High-Temperature Process Heat, Cell Reports Physical Science (2020), https://doi.org/10.1016/j.xcrp.2020.100135



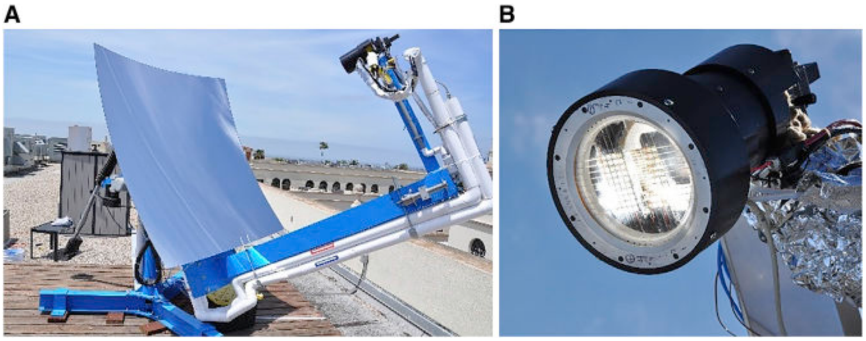


**Figure 6. Outdoor Testing of the Solar Cogeneration System Prototype**
(A) Two-stage tCPV/T receiver mounted at the focal point of a 2.72-$m^2$ parabolic concentrator dish.
(B) Close-up of the tCPV/T module on-sun with concentrated sunlight illuminating the cells in front and the thermal receiver behind.

### *Materials Availability*

This study did not generate new unique reagents.

### *Data and Code Availability*

All of the key data supporting the findings of this study are presented within the article and the Supplemental Information. All other data are available from the Lead Contact upon reasonable request.

## Outdoor System Demonstration

The prototype tCPV/T system is composed of a pedestal mount, azimuth-altitude dual-axis tracker (GST-300), 2.72 $m^2$ square paraboloidal dish mirror with a 45° rim angle and a 1.5-m focal length (4-mm-thick, slumped low-iron float glass, silver back-coated, from REhnu), a single support arm with instrumentation and HTF piping, and the hybrid receiver (Figures 1A and 6). The system was tested over 18 months on the roof of the University of San Diego Shiley-Marcos School of Engineering building. In this time, nine tCPV modules and three thermal receiver iterations were developed and tested, with a steady increase in performance for each iteration. The dish was partially masked in early testing to reduce total flux on the hybrid receiver; flux mapping was used to quantify spatial distribution and intensity on the tCPV receiver (see Supplemental Experimental Procedures). Outdoor test data for the two most recent modules is highlighted in Tables S1–S3. The most recent tCPV/T prototype has been tested for >8 cumulative hours and 2,500 suns-h (product of average concentration over each test and duration of tests). Briefly, the DNI (directly measured with an Eppley NIP [normal incidence pyrheliometer] mounted to the tracker), thermal receiver power, tCPV electric power, and tCPV cooling power are measured throughout the duration of the test, along with temperature monitoring within the tCPV cell array.

## Electrical Characterization

The tCPV module was tested under 1 sun using a solar simulator (AM1.5D spectrum, TS-Space Systems) as well as outdoors in San Diego, California, as shown in Figure 6. Electrical performance was measured using a BK Precision 8514 programmable DC electronic load controlled by custom LabVIEW code. The load performed an IV sweep on the tCPV module every 5 min to calculate a maximum power point setting (current and voltage), fill factor, $V_{oc}$, $J_{sc}$, $R_{shunt}$, and $R_{series}$. In between IV sweeps, the programmable load operated at the max power point setting recording $PV_{elec,power}$ every 15 s. For the module IV sweeps, the variable load used the constant voltage mode. The voltage was swept from 0.6 to 16.5 V, with an initial step size of 1.25 V per step. A logarithmic step size multiplier of 0.94 was applied to shorten each successive voltage step size to add additional data points around the IV curve knee. Each IV sweep was taken over 15 s, with a dwell time per voltage step of 500 ms.

### Life-Cycle Testing

To identify and correct any early failure modes, each module underwent 10 thermal cycles of 25°–110°C, with a dwell time of 30 min at 110°C per cycle, before outdoor testing. Cell temperatures were monitored using thermocouples, with forward bias tests taken between each cycle and IV tests at 1 sun taken before and after the thermal cycling test campaign to assess any degradation. A final 1-h test at 1 sun was performed to confirm the stable operation of all of the module components before beginning the outdoor testing.

### Thermal Power Output and Temperature Monitoring

Four type K 30G bare-wire thermocouples were embedded at various positions in the cell layer of the tCPV module to monitor the temperature of the cells. The total cooling power of the microfluidic cooling system was measured by immersed type K thermocouples mounted to the cooling system inlet and outlet ports, along with an Omega FLR1000 flowmeter. Fluid inlet and outlet pressures were measured using Omega PX309-015GV pressure sensors. The thermal receiver was outfitted with 12 type K thermocouples directly welded to the back (non-irradiated) surface. Additional fluid piping centerline-immersed thermocouples and Omega PX1191KAI pressure transducers were installed at several key locations throughout the HTF loop. The flow rate through the thermal receiver was controlled with a ProMinent Sigma/2 positive displacement metering pump with adjustable stroke and ±1% flow rate accuracy, and measured inline using an Omega FLR1009ST-D flowmeter. An adjustable pressure relief valve downstream of the thermal receiver maintained the pressure of the fluid at the outlet of the receiver. All of the data, except for electrical power performance, were recorded at 15-s intervals using an Agilent 34972A datalogger.

### Transmission Data

Module transmission was also measured using a UV/visible light spectrometer (Ocean Optics, QEPro) and a near-IR (NIR) spectrometer (Ocean Optics, NIRQUEST) coupled to a bifurcated 600-μm fiberoptic cable, and a deuterium-halogen lamp was used as the reference spectrum.

## SUPPLEMENTAL INFORMATION

Supplemental Information can be found online at https://doi.org/10.1016/j.xcrp.2020.100135.

## ACKNOWLEDGMENTS

The information, data, or work presented herein was funded in part by the Advanced Research Projects Agency-Energy, US Department of Energy under award no. DEAR0000473 and the Louisiana Board of Regents under contract no. LEQSF (2018-19)-RD-D-05.

## AUTHOR CONTRIBUTIONS

M.D.E. and D.S.C. jointly supervised the project and developed the core idea. M.D.E., D.S.C., B.R., K.I., Y.V.J., J.R., and C.S. analyzed the data and contributed to the assembly and writing of the manuscript. B.R. led the technoeconomic analysis.

K.I., Y.V.J., and J.R. assembled the transparent CPV modules and performed the lab characterization. D.S.C., C.S., and J.P. assembled the thermal receivers and outdoor testbed and performed the outdoor characterization. D.S.C., C.S., N.G., and F.M. developed the testbed flux mapping process.

## DECLARATION OF INTERESTS

M.D.E., B.R., K.I., Y.V.J., and D.S.C. are named inventors on patent applications (PCT/US2015/038396, PCT/US17/24635, PCT/US18/19782) related to the work presented in this article, which are owned by Tulane University. The remaining authors declare no competing interests.

Received: December 16, 2019
Revised: June 9, 2020
Accepted: June 18, 2020
Published: July 15, 2020

## REFERENCES

1. Calise, F., Cipollina, A., d'Accadia, M.D., and Piacentino, A. (2014). A novel renewable polygeneration system for a small Mediterranean volcanic island for the combined production of energy and water: dynamic simulation and economic assessment. Appl. Energy *135*, 675–693.

2. Rosen, M.A., Le, M.N., and Dincer, I. (2005). Efficiency analysis of a cogeneration and district energy system. Appl. Therm. Eng. *25*, 147–159.

3. Onovwiona, H.I., and Ugursal, V.I. (2006). Residential cogeneration systems: review of the current technology. Renew. Sustain. Energy Rev. *10*, 389–431.

4. Kurup, P., and Turchi, C. (2015). Initial Investigation into the Potential of CSP Industrial Process Heat for the Southwest United States. NREL Tech. Rep. NREL/TP-6A (National Renewable Energy Laboratory).

5. Ni, G., Li, G., Boriskina, S.V., Li, H., Yang, W., Zhang, T., and Chen, G. (2016). Steam generation under one sun enabled by a floating structure with thermal concentration. Nat. Energy *1*, 1–7.

6. Fares, R.L., and Webber, M.E. (2017). The impacts of storing solar energy in the home to reduce reliance on the utility. Nat. Energy *2*, 1–10.

7. Modi, A., Bühler, F., Andreasen, J.G., and Haglind, F. (2017). A review of solar energy based heat and power generation systems. Renew. Sustain. Energy Rev. *67*, 1047–1064.

8. Branz, H.M., Regan, W., Gerst, K.J., Borak, J.B., and Santori, E.A. (2015). Hybrid solar converters for maximum exergy and inexpensive dispatchable electricity. Energy Environ. Sci. *8*, 3083–3091.

9. Chow, T.T. (2010). A review on photovoltaic/thermal hybrid solar technology. Appl. Energy *87*, 365–379.

10. Sharaf, O.Z., and Orhan, M.F. (2015). Concentrated photovoltaic thermal (CPVT) solar collector systems: Part I - Fundamentals, design considerations and current technologies. Renew. Sustain. Energy Rev. *50*, 1500–1565.

11. Sharaf, O.Z., and Orhann, M.F. (2015). Concentrated photovoltaic thermal (CPVT) solar collector systems: part II - Implemented systems, performance assessment, and future directions. Renew. Sustain. Energy Rev. *50*, 1566–1633.

12. Han, X., Zhao, G., Xu, C., Ju, X., Du, X., and Yang, Y. (2017). Parametric analysis of a hybrid solar concentrating photovoltaic/concentrating solar power (CPV/CSP) system. Appl. Energy *189*, 520–533.

13. Michael, J.J., Iniyan, S., and Goic, R. (2015). Flat plate solar photovoltaic-thermal (PV/T) systems: a reference guide. Renew. Sustain. Energy Rev. *51*, 62–88.

14. Weinstein, L.A., McEnaney, K., Strobach, E., Yang, S., Bhatia, B., Zhao, L., Huang, Y., Loomis, J., Cao, F., Boriskina, S.V., et al. (2018). A hybrid electric and thermal solar receiver. Joule *2*, 962–975.

15. He, W., Chow, T.T., Ji, J., Lu, J., Pei, G., and Chan, L.S. (2006). Hybrid photovoltaic and thermal solar-collector designed for natural circulation of water. Appl. Energy *83*, 199–210.

16. Chow, T.T., He, W., and Ji, J. (2006). Hybrid photovoltaic-thermosyphon water heating system for residential application. Sol. Energy *80*, 298–306.

17. Matuska, T. (2014). Performance and economic analysis of hybrid PVT collectors in solar DHW system. Energy Procedia *48*, 150–156.

18. Widyolar, B.K., Abdelhamid, M., Jiang, L., Winston, R., Yablonovitch, E., Scranton, G., Cygan, D., Abbasi, H., and Kozlov, A. (2017). Design, simulation and experimental characterization of a novel parabolic trough hybrid solar photovoltaic/thermal (PV/T) collector. Renew. Energy *101*, 1379–1389.

19. Abdelhamid, M., Widyolar, B.K., Jiang, L., Winston, R., Yablonovitch, E., Scranton, G., Cygan, D., Abbasi, H., and Kozlov, A. (2016). Novel double-stage high-concentrated solar hybrid photovoltaic/thermal (PV/T) collector with nonimaging optics and GaAs solar cells reflector. Appl. Energy *182*, 68–79.

20. Kribus, A., Kaftori, D., Mittelman, G., Hirshfeld, A., Flitsanov, Y., and Dayan, A. (2006). A miniature concentrating photovoltaic and thermal system. Energy Convers. Manage. *47*, 3582–3590.

21. Schmitz, M., Wiik, N., Ambrosetti, G., Pedretti, A., Paredes, S., Ruch, P., Michel, B., and Steinfeld, A. (2017). A 6-focus high-concentration photovoltaic-thermal dish system. Sol. Energy *155*, 445–463.

22. Xu, Q., Ji, Y., Riggs, B., Ollanik, A., Farrar-Foley, N., Ermer, J.H., Romanin, V., Lynn, P., Codd, D., and Escarra, M.D. (2016). A transmissive, spectrum-splitting concentrating photovoltaic module for hybrid photovoltaic-solar thermal energy conversion. Sol. Energy *137*, 585–593.

23. Ju, X., Xu, C., Han, X., Du, X., Wei, G., and Yang, Y. (2017). A review of the concentrated photovoltaic/thermal (CPVT) hybrid solar systems based on the spectral beam splitting technology. Appl. Energy *187*, 534–563.

24. Perl, E.E., Simon, J., Friedman, D.J., Jain, N., Sharps, P., McPheeters, C., Sun, Y., Lee, M.L., and Steiner, M.A. (2018). (Al)GaInP/GaAs Tandem Solar Cells for Power Conversion at Elevated Temperature and High Concentration. IEEE J. Photovolt. *8*, 640–645.

25. Otanicar, T., Dale, J., Orosz, M., Brekke, N., DeJarnette, D., Tunkara, E., Roberts, K., and Harikumar, P. (2018). Experimental evaluation of a prototype hybrid CPV/T system utilizing a nanoparticle fluid absorber at elevated temperatures. Appl. Energy *228*, 1531–1539.

26. Yu, Z.J., Fisher, K.C., Meng, X., Hyatt, J.J., Angel, R.P., and Holman, Z.C. (2019). GaAs/silicon PVMirror tandem photovoltaic mini-module with 29.6% efficiency with respect to the outdoor global irradiance. Prog. Photovolt. Res. Appl. *27*, 469–475.

28. Riggs, B.C., Biedenharn, R., Dougher, C., Ji, Y.V., Xu, Q., Romanin, V., Codd, D.S., Zahler, J.M., and Escarra, M.D. (2017). Techno-economic analysis of hybrid PV/T systems for

CellPress
OPEN ACCESS

Cell Reports
Physical Science
Article

process heat using electricity to subsidize the cost of heat. Appl. Energy *208*, 1370–1378.

29. Xu, Q., Ji, Y., Krut, D.D., Ermer, J.H., and Escarra, M.D. (2016). Transmissive concentrator multijunction solar cells with over 47% in-band power conversion efficiency. Appl. Phys. Lett. *109*, 193905.

30. Robertson, J., Riggs, B., Islam, K., Ji, Y.V., Spitler, C.M., Gupta, N., Krut, D., Ermer, J., Miller, F., Codd, D., and Escarra, M. (2019). Field Testing of a Spectrum-Splitting Transmissive Concentrator Photovoltaic (tCPV). Module. Renew. Energ. *139*, 806–814.

31. Escarra, M.D., Codd, D., Miller, F., Ermer, J., Romanin, V., Riggs, B.C., Robertson, J., Ji, Y., Islam, K., Davis, C., and Woody, M. (2018). A Hybrid CPV/T System Featuring Transmissive, Spectrum-Splitting Concentrator Photovoltaics. In 2018 IEEE 7th World Conference on Photovoltaic Energy Conversion (WCPEC) (A Joint Conference of 45th IEEE PVSC, 28th PVSEC, and 34th EU PVSEC) (IEEE), pp. 1658–1660.

32. Ji, Y., Xu, Q., Riggs, B., Islam, K., Ollanik, A., Ermer, J.H., Krut, D.D., Romanin, V., Codd, D., and Escarra, M.D. (2017). Optical Design and Validation of an Infrared Transmissive Spectrum Splitting Concentrator Photovoltaic Module. IEEE J. Photovolt. *7*, 1469–1478.

33. Vorobiev, Y., González-Hernández, J., Vorobiev, P., and Bulat, L. (2006). Thermal-photovoltaic solar hybrid system for efficient solar energy conversion. Sol. Energy *80*, 170–176.

34. Vorobiev, Y.V., González-Hernández, J., and Kribus, A. (2006). Analysis of potential conversion efficiency of a solar hybrid system with high-temperature stage. J. Sol. Energ. Eng. *128*, 258–260.

35. Dimri, N., Tiwari, A., and Tiwari, G.N. (2019). Comparative study of photovoltaic thermal (PVT) integrated thermoelectric cooler (TEC) fluid collectors. Renew. Energy *134*, 343–356.

36. Dimri, N., Tiwari, A., and Tiwari, G.N. (2017). Thermal modelling of semitransparent photovoltaic thermal (PVT) with thermoelectric cooler (TEC) collector. Energy Convers. Manage. *146*, 68–77.

37. Tiwari, G.N., and Gaur, A. (2014). Photovoltaic thermal (PVT) systems and its applications. In 2nd International Conf. on Green Energy and Technology (IEEE), pp. 132–138.

38. Islam, K., Riggs, B., Ji, Y., Robertson, J., Spitler, C., Romanin, V., Codd, D., and Escarra, M.D. (2019). Transmissive Microfluidic Active Cooling for Concentrator Photovoltaics. Appl. Energy *236*, 906–915.

39. Khalil, I., Hayes, R., Pratt, Q., Spitler, C., and Codd, D. (2018). Experimental and numerical modeling of heat transfer in directed thermoplates. Int. J. Heat Mass Transf. *123*, 89–96.

40. Khalil, I., Pratt, Q., Spitler, C., and Codd, D. (2019). Modeling a thermoplate conical heat exchanger in a point focus solar thermal collector. Int. J. Heat Mass Transf. *130*, 1–8.

41. California Public Utilities Commission. (2018). Zero Net Energy https://www.cpuc.ca.gov/zne/.